Current Science
CS 5 (5), 4730-4744 (2025)
Received 19 July 2025 | **Revised 10 August** 2025 | **Accepted 15 September** 2025 | **Online Available 10 October** 2025
https://doi.org0/10.52845/CS/2025-5-5-31

Current Science

Current Science

OPEN ACCESS

ISSN(O)2795-8639

Research Article

Optimization Design and Experimental Study of Bionic Rotating Blades of Tobacco Field Rotary Tillers Based on EDEM and RSM

Ting Guo[1]*, Wujin Li[1], Shuguang Peng[2], Wen Li[1], Xianglu Gong[3]

[1]Chenzhou City Company, Hunan Province Tobacco Company, Chenzhou, 423000, P.R. China

[2]Hunan Province Tobacco Company, Changsha, 410007, P.R. China

[3]Collegeof Engineering and Technology, Southwest University, 400100, P.R. China

[*]Corresponding Author: Xianglu Gong

Abstract:
To design a high-performance rotating tiller suitable for local tobacco-growing regions, this study developed a bionic rotating blade based on the foreleg curve of the dung beetle and established a reliable discrete element model (DEM) for the soil in tobacco fields. A soil-throwing motion model of the blade was constructed, and its strength was verified under extreme working conditions to ensure stability and reliability. Field operation simulations were conducted using the EDEM, focusing on the effects of blade type, forward speed, and rotational speed through single-factor and multi-factor experiments. The results showed that the influences of these factors are significant. The accuracy of the EDEM soil model was verified by determining the optimal parameters using the response surface method (RSM). Soil overturning efficiency and particle motion patterns were analyzed using optimal parameters. Field tests confirmed the reliability of the simulations, and the relative error between the physical and simulation results was below 10%. This study provides detailed theoretical guidance for the design of rotary tillers in tobacco producing regions.

Keywords: Bionic Design; Discrete elements; Optimal Combination Parameters; State Volume Analysis.

1. Introduction

Tobacco (*Nicotiana tabacum L.*) is an angiosperm, an annual or limited perennial herbaceous plant in the Solanaceae family. It originates from South America and is widely cultivated in Chinese provinces, serving as a critical economic crop in the region [4,15]. Due to its unique economic value, tobacco was introduced to China in earlier centuries, and its production has continued to grow over time[1]. In 2023, the planting area of tobacco cultivation was 1,084 million hectares, and the planting area continued to increase year by year[9]. Tobacco cultivation has significantly increased rural income, reduced poverty, and promoted local economic development in southern China[5]. However, labor migration to urban areas has limited the expansion of tobacco agriculture, which emphasizes the urgent need for efficient, high-performance, and cost-effective agricultural machinery. Tillage is one of the most critical operations in tobacco production, yet the availability of specialized equipment remains limited[11].

The application of numerical simulations has grown significantly in agricultural research[3,9]. Simulation transforms the real problem into computational problems, which can save time and resources when the theoretical model is accurate[2,7]. Ucgul and Saunders (2020) analyzed the performance of the molar plate plough using the discrete unit method (DEM) to achieve the accurate prediction of traction force and vertical tillage force. Mudarisov et al. (2019) modeled the

soil-cutting process using Newtonian rheological theory, providing insights into soil-tool interactions. In conclusion, it is feasible to optimize the tools and make detailed analysis with certain advantages[16].

Bionic design principles inspired by natural evolution also provide valuable references for mechanical innovation. Zhu et al. (2022) developed a bionic rotating blade mimicking the combined digging and soil-throwing motion of mole crickets, thus improving performance. Similarly, Xiao et al. (2021) designed a bionic rotating tiller based on Gryllotalpa orientalis, which reduced the horizontal and vertical resistance by 9.91% and 9.09%, respectively.

Despite these advances, the design of most tobacco machinery is still limited to physical prototyping and field testing, lacking rigorous theoretical research. This approach often leads to material waste and inefficiency. To address these challenges, this study integrates previous results from rotary tillering studies and applies DEM to simulate soil-tool interactions. A bionic blade inspired by forelegs of dung beetle was designed, and the soil model of tobacco fields was developed. The optimal leaf surface (RSM) parameters were determined by the response surface method, which provides a theoretical basis for understanding the mechanism of soil tillage and the key influencing factors. This study aims to provide strong theoretical support and practical validation for the design and development of rotary tiller in tobacco.

1. Materials and Methods

2.1 Design of the Working Component

2.1.1 Bionic Curve Fitting

Structural traits inherited through evolution often demonstrate exceptional adaptability, making them valuable references for engineering design. Studies have shown that mimicking the structures of Gryllotalpa orientalis and rabbit claw toes can effectively optimize the design of rotary tiller blades, yielding significant performance improvements[12]. To meet the specific requirements of small-scale rotary tillers in hilly regions—such as soil loosening, low energy consumption, effective soil-throwing, and structural simplicity—this study selected the digging and soil-lifting motions of dung beetle forelegs as a bionic design reference to enhance component performance.

The geometric curve of the dung beetle foreleg was extracted using reverse engineering and image processing techniques. High-resolution images of the foreleg (Fig. 1.1) were processed using OpenCV for grayscale conversion (Fig. 1.2) and binarization (Fig. 1.3) to generate the foreleg's contour curve (Fig. 1.4). The curve's coordinate data were imported into Origin software and fitted by the least squares method. An ALLometric function was applied to derive the bionic curve equation:

$$Y = 251.49 - (-993.52) \times 0.99^{x} \quad (1)$$

The fitting accuracy was determined by the coefficient of determination R2=0.99672, indicating high accuracy. This bionic curve provides a reference for designing the working component.

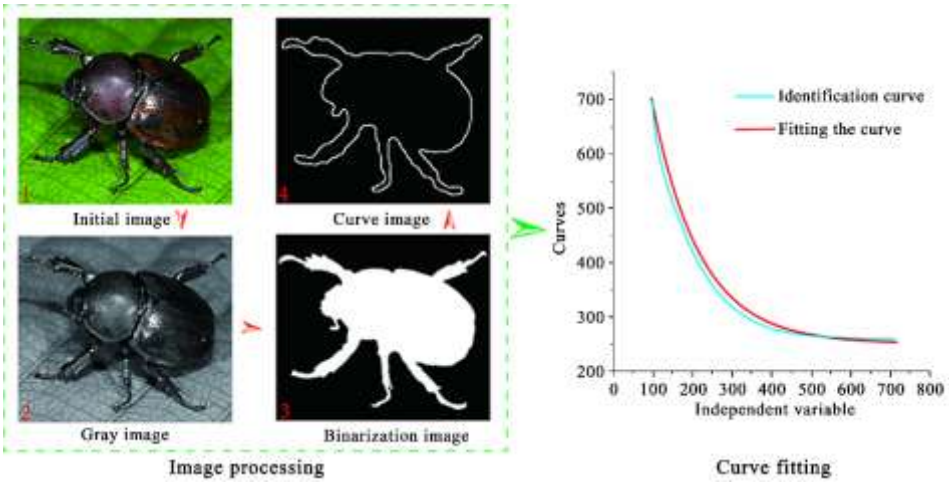

Figure 1. Schematic diagram of bionic action and foreleg curve fitting.

2.1.2 Bionic Design of the Working Component

Based on the fitted bionic curve of dung beetle forelegs, the design incorporated this curve into the side blade of the rotary tiller. The cutting and soil-lifting functions of dung beetle forelegs are highly similar to the working principles of rotary tiller blades. By applying the bionic curve, the cutting and soil-throwing performance of the blade was enhanced. The remaining blade structures were designed in accordance with international rotary tiller standards to ensure operational reliability and consistency.

The traditional rotary tiller is mainly composed of a handle, a side blade surface, a transition blade surface and a front blade surface. The side blade surface is mainly used to cut soil and remove surface straw or weeds, while the front blade surface is responsible for cutting, crushing and turning soil (Feng et al., 2024; Khalid et al., 2022). The trajectory of the rotary tiller is a cycloidal motion, which is a composite of circular and linear motion, and its trajectory shape is controlled by the speed ratio (Zhang et al., 2024). Based on the functional characteristics of dung beetle forelimbs for cutting and digging, this study applies the fitted bionic curve to the side blade design of the rotary tiller, and improves the soil cutting and throwing performance through bionic scaling and optimization[16].

The rotating blades designed in this study had a rotation radius of 245 mm. The material is high strength steel, which meets the requirements of GB/T 5669-2008, ensuring durability and strength. A 3D model of the blades was created in SolidWorks 2023 and further analyzed using Simulia software. This model not only guided the manufacturing process, but was also used in EDEM simulations to evaluate the effectiveness of the bionic design (Fig. 2).

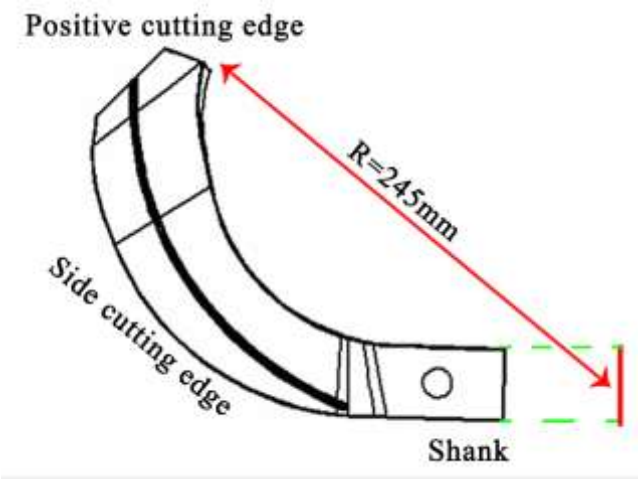

Figure 2. Schematic diagram of rotary tiller

2.1.3 Static Analysis

Due to the good formability and high toughness of the selected material, under normal circumstances, the consumption of the cutting roller is natural wear, but it is not ruled out that sometimes there will be stones in the soil, directly hitting the cutting roller, resulting in its crushing. The finite element analysis software ABAQUS is used to perform numerical simulation analysis on the mechanical properties of the working cutter roller, and the designed working parts are studied under extreme working conditions to obtain the limit state quantity in advance, and the above situation is avoided through structural design and material selection.

The specific movement of the working part is rotation forward, the maximum design speed of 300rpm is selected as the simulation speed, and the forward speed is 1.2m·s-1. Since the working part is wheeled, the impact mode of the stone in the soil is rotation impact, as shown in Fig. 3. Since the hardness of the stone is much higher than that of the knife roller, the stone is set as a rigid body.

Figure 3.Finite element static analysis of the rotary blade.

2.1.4 Development of the DEM Model

Combined with the actual soil distribution in the flue-cured tobacco planting area, the three-layer soil model of the tillage layer, plough layer and core soil layer was established by discrete unit method to prepare for the subsequent virtual simulation test of the tillage machine. In this paper, the discrete element software EDEM is used to conduct a deep loosening and shoveling simulation test to establish a suitable soil contact model. At the same time, in order to accurately reflect the performance of the working parts of the soil-raising machine, the discrete element simulation parameters need to be determined.

Soil Model

Existing research and field investigations have shown that soil particles can be mainly divided into block, core, flake and columnar particles(Tekeste et al., 2020). In order to better simulate the real soil conditions, four approximate soil model particles were established through the spherical particle accumulation function of EDEM. A single spherical model approximates block particles, three spherical models in parallel represent approximate core particles, a triangular arrangement of three spherical models approximates flake particles, and a stack of four spherical models approximates columnar particles. The radius of each spherical model is set to 3 mm. The particle models are shown in Figure 3, and the spatial position coordinates of each spherical particle are shown in Table 1. The ratio of block particles: core particles: flake particles: columnar particles in the soil is approximately 34:26:20:20. The model radius of each particle is set to a normal distribution with a mean of 1 and a standard deviation of 0.05.

Soil particle model		Particle radius /mm	Coordinates of the spatial position of the particle center		
			X	Y	Z
Massive model	particle 1	3	0	0	0
Nucleated model	particle 1	3	3	0	0
	particle 2	3	-3	0	0
	particle 3	3	0	0	0
Sheet-shape grain	particle 1	3	2	-1	0
	particle 2	3	0	3	0
	particle 3	3	-2	-1	0
Columnar grain	particle 1	3	2	-1	0
	particle 2	3	0	3	0

	particle 3	3	-2	-1	0
	particle 4	3	0	0	4

Table 1.Parameters of soil particle model

The soil container was modeled as a box measuring 1500 × 400 × 450 mm, divided into three layers: the top layer (L1, 0–8 cm), the plow layer (L2, 8–20 cm), and the core layer (L3, 20–30 cm). Approximately 1.2 million particles were generated to fill the container, simulating realistic soil conditions (Fig. 4).

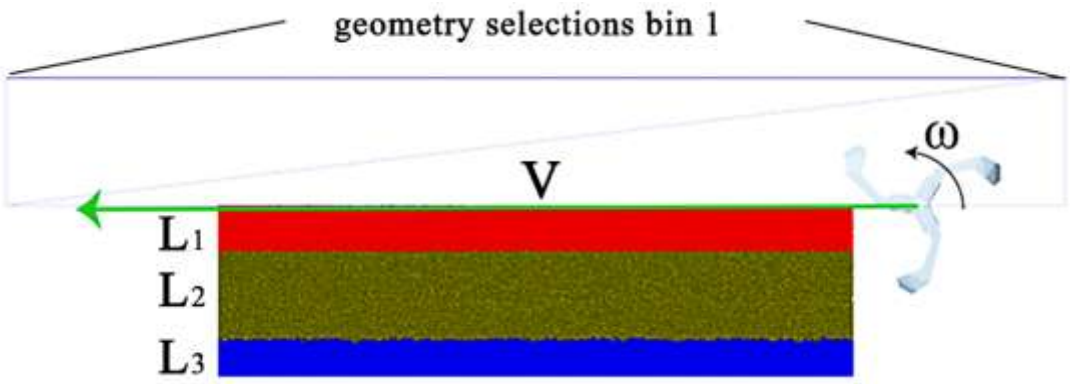

Figure 4. Soil model structure in EDEM.

2.2 Contact Model

The contact model is based on the changes in the shape and state of soil particles under external forces under static conditions. The force and performance of the rotary tiller are an embodiment of the contact model. During the operation of the rotary tiller, soil particles are mainly acted upon by two forces, namely the gravity Mg of the particles themselves and the external force F-resultant force between the particles. This force may be the contact force between the particles or the force generated by the collision and friction with the rotary tiller. According to Newton's second law of motion, the equations of linear motion and rotation of particles are(Johnson et al., 1997),

$$\begin{cases} m_i \frac{\mathrm{d}v_i}{\mathrm{d}t} = m_i g + \sum_{j=1}^{n_i} \left(F_{n,ij} + F_{n,ij}^{l} + F_{\tau,ij} + F_{\tau,ij}^{d} + F_{coh,ij}\right) \\ I_i \frac{\mathrm{d}w_i}{\mathrm{d}t} = \sum_{j=1}^{n_i} \left(T_{\tau,ij} + T_{r,ij}\right) \end{cases} \quad (2)$$

$$F_{coh,ij} = k_{coh,ij} A_{coh,ij} \quad (3)$$

Where $\boldsymbol{I_i}$ is the moment of inertia of particle i; ni is the total number of particles contacted by particle *i*, v_i is the moving velocity of particle i, mm·s^{-1}; w_i is the angular velocity of particle *i*, rad·s^{-1}; $\boldsymbol{T_{\tau,ij}}$ is the torque formed by the tangential force on particle *i*; $\boldsymbol{T_{r,ij}}$ is the rolling moment of particle *i*; $\boldsymbol{F_{coh,ij}}$ is the normal binding force, N; $\boldsymbol{k_{coh,ij}}$ is adhesion energy density; $\boldsymbol{A_{coh,ij}}$ is particle contact area, mm^2.

The JKR contact model(Wu and You, 2007) introduces the surface energy into the interparticle interaction, which can well simulate the interparticle cohesion caused by water. Therefore, the JKR model is used for both the tillage layer L1 and the plow layer L2.

JKR contact model is a viscous contact model based on the Hertz contact theory combined with the JKR theory. It is suitable for considering the influence of van der Waals forces in the contact area and simulating viscous systems, such as dry powder or wet particles. Compared with the Hertz-Mindlin contact model, its advantage is that the calculation of the JKR normal elastic force is based on the overlap δ, interaction parameters and surface energy γ:

$$F_{JKR} = -4\sqrt{\pi\gamma E^*}\alpha^{\frac{3}{2}} + \frac{4E^*}{3R^*}\alpha^3 \quad (5)$$

$$\delta = \frac{\alpha^2}{R^*} - \sqrt{\frac{4\pi\gamma\alpha}{E^*}} \quad (6)$$

where F_{JKR} is the normal elastic force, N; α is the radius of the contact circle of two particles in contact with each other, m; δ is the overlap quantity, m; γ is the surface energy, N/m; E* is equivalent elastic modulus, MPa; R* is the equivalent radius, m. The equivalent elastic modulus and equivalent radius are defined as:

$$\frac{1}{E^*} = \frac{1-{v_i}^2}{E_i} + \frac{1-{v_j}^2}{E_j} \quad (7)$$

$$\frac{1}{R^*} = \frac{1}{R_i} + \frac{1}{R_j} \quad (8)$$

where E_i, v_i, R_i and E_j, v_j, R_j are the elastic modulus, Poisson's ratio and particle radius of two particles in contact, respectively.

To ensure the authenticity of the simulation results, the soil model parameters were reasonably set according to the different layers of the soil in the flue-cured tobacco planting area. For the tillage layer (L1) and the plow bottom layer (L2), the JKR model with cohesive characteristics was used to simulate the relatively soft upper soil; for the soil core layer and bottom layer (L3), the Hertz-Mindlin with bonding model was used to simulate the relatively solid lower soil. Combined with relevant research results, the soil model parameters are detailed in Table 2.

Table 2.Parameters of soil simulation model

Parameter		Numerical Value
Poisson’s ratio of soil particles		0.38
Soil particle density (kg· m^{-3})		2680
Shear modulus of soil particles (Pa)		1200000
Soil-soil coefficient of recovery		0.55
Soil-soil static friction coefficient		0.84
Soil-soil dynamic friction coefficient		0.1
JKR surface energy (J· m^{-2})		12.73
Bonding model parameters	Normal stiffness coefficient (N· m^{-3})	2400000
	Tangential stiffness coefficient (N· m^{-3})	1700000
	Critical normal stress (Pa)	235000
	Critical tangential stress (Pa)	186000

2.2.1 Boundary Conditions

Based on EDEM, the working parts of rotary tiller are simulated factors, and the boundary conditions are set as follows. According to 2.1.2, the rotary tiller roller is designed, and the rotary tiller roller is drawn by SOLIDWORKS. It is combined and fixed according to the actual situation, and three are grouped. The working parts are saved in .igs format. In EDEM, an uncovered soil trough is

created with a length, width and height of 400×2000×300mm.

Import the roller .igs format into EDEM, and adjust the position, rotation and other components to align it with the soil model in the working posture. According to the actual working state, two movements are set for the working parts, one is the linear movement V, and the other is the rotation ω of the rotary tiller disc along the center of mass rotation axis, to simulate the rotation of the roller when the earthmoving machine is working, cutting soil and throwing soil. The specific values of these two movements are determined according to the specific requirements of the test. The tool material is set to 65Mn, and the specific parameters are shown in Table 3.

Table 3.Steel related simulation parameters

Parameter	Numerical Value
Poisson's ratio of 65Mn	0.35
The density of steel (kg·m^{-3})	7830
Shear modulus of steel (Pa)	7.27×1010
Coefficient of restitution between 65Mn and soil	0.3
Coefficient of static friction between 65Mn and soil	0.6
Coefficient of dynamic friction between 65Mn and soil	0.1

Under the premise of ensuring the continuous movement of soil particles during the simulation, the fixed time step was set to 3.98477E-05s, and the total simulation time was based on the trough length / line speed, which is suitable for the full-length soil model with complete action. The time is about 2~7s, and the grid unit size is 3 times the minimum particle radius, which is 3.825mm in this simulation.

During post-processing, the reaction force between the cutter disc and all particles during operation is obtained through data output, and the maximum value is recorded. A geometric selection bin 1 with a height of 100mm is set at the top of the soil trough, and the number of particles passing through the plane is recorded to obtain the soil removal amount of the rotating cutter roller and evaluate the soil removal performance.

2.3 Experimental Design

2.3.1 Single-Factor Experiment

Design parameters for the rotary tiller were determined based on agricultural standards for small-scale equipment. Preliminary tests established a rotational speed range of 150–350 rpm and a forward speed of 1–5 km·h-1. Excessive speed led to energy waste and machine instability, while lower speed caused insufficient soil cutting. Forward speed below 1 km/h reduced efficiency, while speeds above 5 km·h-1 impacted maneuverability in tobacco fields.

The best match between the rotational speed and the forward speed was identified as a key design indicator. Statistical methods were used to explore the relationship between these parameters and the running performance.

2.3.2Multi-Factor Experiment

The single-factor test preliminarily optimized the advance speed and rotation speed of the tiller cutter plate, but only obtained whether the corresponding specifications can achieve the purpose of soil lifting. The research on its effect and various indicators is not sufficient, and the optimal value has not been obtained. Therefore, the BBD (Box-Behnken) orthogonal rotation combination test is designed, and the factor level coding table is shown in Table 4. With the forward speed, rotation speed, and cutter shape as the influencing factors, and the resistance of a single component and the amount of soil lifted as the corresponding indicators, a regression model is established to solve the optimal parameter combination of the rotary tillage components of the rotary tiller.

Blade types included a conventional rotary blade (Type 4), a bionic blade based on dung beetle forelegs (Type 5), and a widened rotary blade (Type 6). Factor levels and coded values are listed in Table 4.

Table 4.Factors and levels of simulation test

	Factors	-1	0	1	Δj
X_1	Rotation speed /r·min^{-1}	150	250	350	15
X_2	Advance speed /m·s^{-1}	0.4	0.8	1.2	0.4
X_3	Tool Type	4	5	6	6

2.4 Field Validation

In order to verify the reliability of the simulation model, a rotary tillage blade with optimized structural parameters was developed and tested on November 15, 2024. Since it was not the fertilization period for flue-cured tobacco planting, one-year uncultivated soil consistent with the soil conditions of the tobacco planting area was selected. The soil used in the test was consistent with the simulation type, all of which were clay soils. Before the test, weeds and foreign objects in the test field were cleaned and the test field was leveled to prevent any impact on the test. The main tools include a stopwatch, an electronic scale with an accuracy of 0.01g, a cowhide bag, a tape measure, a ruler, a soil firmness meter, etc. A series of field verification experiments were carried out using a tillage device configured in accordance with the optimal simulation results (Fig.5), and the tool resistance was verified using a stress-strain test piece. Before each test, the speed was measured by a passive magnetoelectric speed sensor, and the test was carried out after the speed was kept consistent with the test requirements. The total test operation stroke was 50m, of which the test stroke was 30m, and 10m was reserved for the front and back strokes. Unit soil dumping amount: The measurement points were evenly divided (each point was 10 cm apart) and the unit soil dumping amount within the unit distance was collected. The soil in the dumping area was collected using kraft paper and its weight was measured using an electronic scale after peeling. A tillage test was also conducted. The experiment was repeated 5 times.

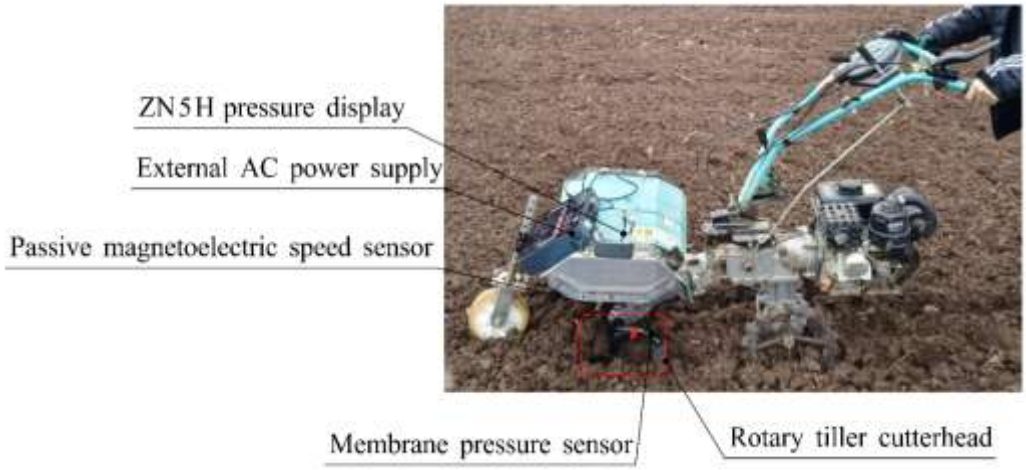

Figure 5. Field test platform

According to the provisions of GB/T5668-2017 Rotary tiller, the rotary tillage performance is tested. When measuring the tillage depth, it is necessary to first clean the soil at the bottom of the ditch and its surroundings, and then put a ruler between the original surface and the intersection of the two ditch walls, and measure the length from the center line of the ditch bottom to the ruler to determine the rotary tillage depth. When measuring, measure one point on the left and right every 2m along the forward direction of the unit. The total number of measurement points for each stroke is not less than 20 points. Calculate according to formula (9):

Average tillage depth of the stroke

$$a_j = \frac{\sum_{i=1}^{a_j} a_{ji}}{n_j} \quad (9)$$

where a_j is the average tillage depth of the *j-th* stroke, cm; a_{ji} is the tillage depth value of the *i*-th point in the *j*-th stroke, cm; n_j is the number of measurement points in the *j*-th stroke.

The ditch width is measured at the same measuring point as the depth, and the test results are calculated according to the method specified in formula (9) to obtain the average width of the rotary tillage within the stroke. The ditch shape in this improved design is required to be rectangular, and only the ditch surface width is measured.

3. Results and Discussion

3.1 Stress Analysis

In view of the extreme working conditions of the rotary tiller, the finite element method was used to simulate the working conditions and the stress distribution of each part of the rotary tiller blade was obtained, as shown in Figure 6. According to the distortion energy density theory, the main factor affecting the plastic yield of the material is the distortion energy density. When the distortion energy density υdw reaches a certain limit value υ0 dw, the material yields. At this time, according to the yield limit value under each stress state in the following formula,

$$\boldsymbol{U_{dw}} = \frac{\boldsymbol{1+\mu}}{\boldsymbol{6E}}[(\boldsymbol{\sigma_1 - \sigma_2})^2 + (\boldsymbol{\sigma_2 - \sigma_3})^2 + (\boldsymbol{\sigma_3 - \sigma_1})^2] = \frac{\boldsymbol{1+\mu}}{\boldsymbol{3E}}\boldsymbol{\sigma_o^2} \quad (10)$$

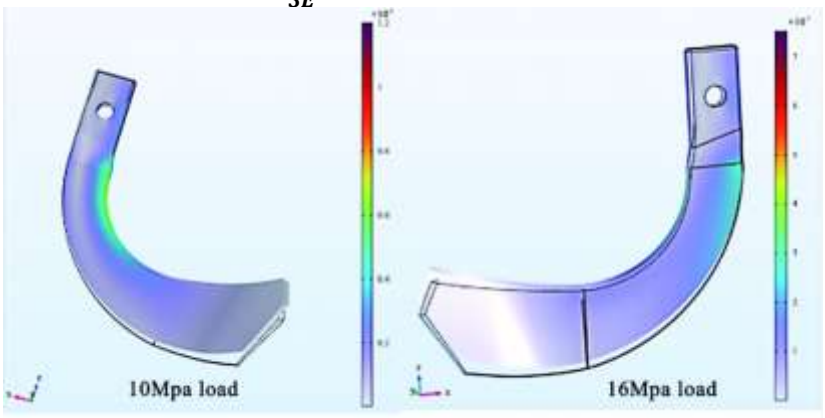

Figure 6 .Stress distribution cloud diagram

Where *Udw* is the distortion energy density MPa; *E* is the elastic modulus of the material, MPa; μ is Poisson's ratio of material; σ1 is the first principal stress, MPa; σ_2 is the second principal stress, MPa; σ_3 is the third principal stress, MPa; σ_o is the yield strength of the material, MPa.

It is worth noting that for the complex states of principal stresses σ_1, σ and σ_3 the distortion energy density formula is as follows,

$$\boldsymbol{v_{dw}} = \frac{\boldsymbol{1+\mu}}{\boldsymbol{6E}}[(\boldsymbol{\sigma_1 - \sigma_2})^2 + (\boldsymbol{\sigma_2 - \sigma_3})^2 + (\boldsymbol{\sigma_3 - \sigma_1})^2] \quad (11)$$

The yield criterion expressed by the stress in Equations (8) and (9) is as follows,

$$\boldsymbol{\sigma} = \sqrt{\frac{\boldsymbol{1}}{\boldsymbol{2}}[(\boldsymbol{\sigma_1 - \sigma_2})^2 + (\boldsymbol{\sigma_2 - \sigma_3})^2 + (\boldsymbol{\sigma_3 - \sigma_1})^2]} \leqslant \boldsymbol{\sigma_o} \quad (12)$$

Finite element simulations identified stress distribution across the rotary blade under extreme working conditions. Maximum equivalent stress occurred at the blade's curved section, with a peak

of 75 MPa under a load of 10 MPa. This value was well below the allowable stress of 120 MPa. Simulations indicated that the blade could withstand operational loads safely, but extreme loads above 16 MPa approached the material's yield point, suggesting room for material improvement.

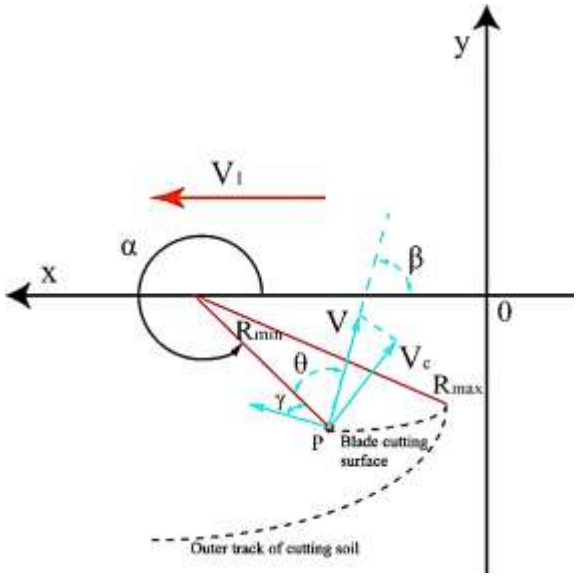

Figure 7. Schematic diagram of soil lifting model mechanism

3.2 Soil-Throwing Model Analysis

The tillage effect of a soil tiller is the most basic functional index requirement of the machine. It has been directly studied as an experiment in 2.3. The influence of three key factors on this index was explored experimentally with some interaction mechanism. The following is a specific quantitative study of the soil tillage process from the aspects of soil particle force and movement.

When the device interacts with the soil, the rotary tillage roller first cuts the soil. After the cutter disc is inserted into the soil, there is a certain amount of soil on the blade surface and the cutting surface. With the continuous translation and rotation of the cutter disc, the thrown soil obtains a certain initial velocity V, and then leaves the cutter disc to realize the tillage action.

In Fig. 6, the angle between the maximum radius *R*max and the minimum radius *R*min of the rotary tillage disc is θ, the angle between the tangent at the end of the positive section and the minimum radius is ψ, and the angle between the absolute speed and the minimum radius is β. Point P is the soil particle that is about to be thrown out when the blade cuts. It moves to the end of the positive section and establishes a motion system at the starting point of the cutting edge. Taking the soil block at point P as the moving point, its initial velocity is the composite motion of the mechanical forward motion and the rotary motion of the cutter roller, and the deceleration motion with only one gravity acceleration after being thrown out. Moreover, the blade starts to break and throw the soil only when the rotation angle is greater than 3π/2. Then the critical initial velocity of the soil particles can be calculated,

$$\begin{cases} \boldsymbol{v = v_c\sqrt{2(1-\sin\gamma)}} \\ \boldsymbol{\beta = \alpha - \theta - 180} \end{cases} \quad (13)$$

The coordinates of the soil particle when it is about to leave the front section of the blade are as follows:

$$\begin{cases} \boldsymbol{x_0 = v_m\frac{\alpha}{\omega} - r\cos\alpha} \\ \boldsymbol{y_0 = r\sin\alpha} \end{cases} \quad (14)$$

Assuming that the moment of throwing soil is t = 0, the initial velocity and direction of the soil particles accelerated and thrown out of the end of the positive section can be determined. The

position of throwing soil can be determined according to formula (14), and the motion trajectory of the submerged soil can be determined according to the following formula:

$$\begin{cases} x = x_0 + v_x t \\ y = y_0 + v_y t - \frac{1}{2} g t^2 \end{cases} \quad (15)$$

x_0 and y_0 are the coordinates of the initial position of the object being thrown, and the initial velocity in the directions of *Vx* and *Vy* is the gravitational acceleration *g*.

3.3 Orthogonal Experiment Results

The simulation experiments followed the parameters in Table 4, with soil cutting resistance (Y_1) and soil-throwing volume (Y_2) as evaluation indicators. Each test was repeated five times, and average values were used after excluding outliers. The results are summarized in Table 5.

Table 5. BBD matrix and experimental responses

	Factors			Responses	
Group	X_1 (rad·min^{-1})	X_2 (m·s-1)	X_3	Y_1 (N)	Y_2
1	250	0.40	4.0	190.5	16942
2	150	1.20	5.0	103.1	10515
3	350	0.80	6.0	141.7	29336
4	250	1.20	4.0	229.4	13883
5	150	0.80	6.0	169.9	12242
6	250	0.80	5.0	112	21396
7	250	0.80	5.0	120.6	20354
8	250	1.20	6.0	143.2	18148
9	350	0.40	5.0	112.14	38493
10	250	0.40	6.0	160.3	28998
11	250	0.80	5.0	129.5	23358
12	350	0.80	4.0	188.3	21805
13	250	0.80	5.0	131.65	22984
14	150	0.80	4.0	143.7	7754
15	250	0.80	5.0	109.2	21364
16	150	0.40	5.0	120.9	14315
17	350	1.20	5.0	140.4	25013
Repeated times of experiments at each level :5 X_1: Rotation speed; X_2: Advance speed; X3: Tool Type; Y_1: Forward resistance, N; Y_2: Total number of soil lifts.					

The results of the variance analysis of the Y1 and Y2 models are shown in Table 6. The results show that the regression model is very significant (P<0.01). For the Y1 model, the P value is <0.01 and the F value is 8.38. Compared with the pure error, the P value is 0.1107, which is not significant. The calculated R2 value is 91.5%, which further confirms the significance of the model and indicates that the model can predict 91.5% of the variability in the response.

The results of the variance analysis of the regression model (Table 6) show that for the linear terms X_1, X_2, X_3 of the Y1 model, the quadratic terms X_1^2 and X_2^2 have significant regression coefficients, and the interaction term coefficient is not significant; the same method analysis shows that the linear terms X_1, X_2, X_3, and the quadratic term X_2^2 of the Y2 model have significant regression coefficients, and the interaction term X_1X_2 is significant (P<0.05).

Table 6.ANOVA results for the fitted regression models of Y_1 and Y_2

Source	Sum of Squares	Degree of freedom	Mean Square	F Value	p-value	
Y_1						
Model	17148.37	9	1905.37	8.38	0.0052**	significant
X_1	252.45	1	252.45	1.11	0.3270	
X_2	130.09	1	130.09	0.57	0.4741	
X_3	2339.28	1	2339.28	10.29	0.0149	
X_1X_2	530.38	1	530.38	2.33	0.1705	
X_1X_3	1324.96	1	1324.96	5.83	0.0465*	
X_2X_3	784.00	1	784.00	3.45	0.1057	
X_1^2	482.29	1	482.29	2.12	0.1886	
X_2^2	360.07	1	360.07	1.58	0.2486	
X_3^2	10956.95	1	10956.95	48.19	0.0002**	
Residual	1591.73	7	227.39			
Lack of Fit	1186.50	3	395.50	3.90	0.1107	not significant
Pure Error	405.23	4	101.31			
Cor Total	18740.10	16				
R^2=91.5%; C.V. %=10.48						
Y_2						
Model	9.254E8	9	1.028E+008	42.20	< 0.0001**	significant
X_1	6.094E8	1	6.094E+008	250.11	< 0.0001**	
X_2	1.216E8	1	1.216E+008	49.91	0.0002**	
X_3	1.004E8	1	1.004E+008	41.21	0.0004**	
X_1X_2	2.343E7	1	2.343E+007	9.61	0.0173*	
X_1X_3	2.315E6	1	2.315E+006	0.95	0.3622	
X_2X_3	1.517E7	1	1.517E+007	6.23	0.0413*	
X_1^2	2.418E6	1	2.418E+006	0.99	0.3523	
X_2^2	3.805E6	1	3.805E+006	1.56	0.2516	
X_3^2	4.723E7	1	4.723E+007	19.38	0.0031**	
Residual	1.706E7	7	2.436E+006			
Lack of Fit	1.082E7	3	3.608E+006	2.32	0.2174	not significant
Pure Error	6.232E6	4	1.558E+006			
Cor Total	9.425E8	16				
R^2=98.19%; C.V.% =7.65						
X_1^2, X_2^2 and X_3^2: quadratic terms of regression model; X_1X_2 , X_1X_3 and X_2X_3: interactive term of regression model. Asterisks indicate significant difference at the (*) 95% and (**) 99% confidence levels.						

At the maximum value of working resistance of Y_1, the interaction effect is obvious, and the trend is consistent with the cutterhead force model; similarly, the order of influence of soil uplift in model Y_2 is $X_3>X_2>X_1$, and both the interaction effect and the quadratic effect have excellent performance.

3.4 Response Surface Analysis

According to the data samples in Table 5 and Table 6, the quadratic polynomial regression model of maximum working resistance and soil uplift was obtained using Design-Expert 13.0 software.

Y_1=120.59+5.62×X_1+4.03×X_2-17.10×X_3+11.51×X_1×X_2+18.2×X_1×X_3-14.0×X_2×X_3-10.7×X_1^2+9. 25×X_2^2+51.01×$X_3^2$$Y_2$=21891.2+8727.6×$X_1$-3898. 63×$X_2$+3542.50×$X_3$-2420×$X_1$×$X_2$+760.75×$X_1$×$X_3$-1947.75× X_2× X_3-757.85× X_1^2 +950.65× X_2^2-3349.10× X_3^2

where Y_1 is the maximum working resistance, N; Y_2 is the amount of soil lifted; X_1 is the rotation speed, rad·min^{-1}; X_2 is the forward speed, m·s^{-1}; X_3 is knife shaped.

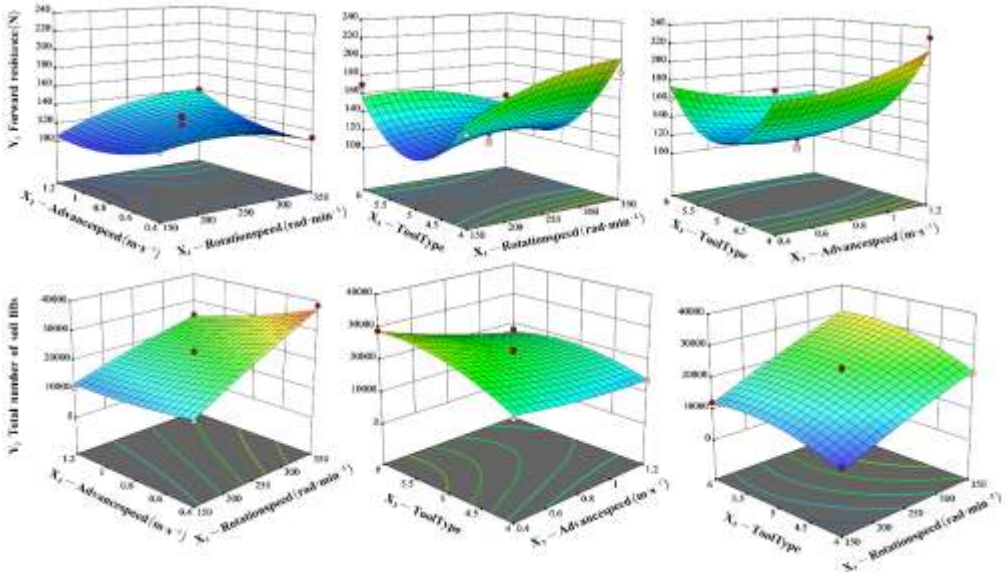

Figure 8. Response surface plots for cutting resistance and soil-throwing volume

Response surface plots (Fig. 8) illustrated interactions among parameters. Increasing the forward speed increased cutting resistance but decreased soil-throwing volume due to reduced contact time. Higher rotational speed positively influenced both indicators, with bionic blade Type 5 achieving superior performance. Optimal parameters were determined as 350 rpm rotational speed, 0.4 m/s forward speed, and bionic blade Type 5, yielding cutting resistance of 107.2 N and soil-throwing volume of 37,965 particles.

3.5 Field Validation

Field verification experiment showed that the tillage depth was 253.1 mm, the average tillage width was 103.22 mm, the field test working resistance was 109.28 N, and the unit soil mass was 2427 g. The measured working resistance was 107.2 N, and the relative error was 1.94% compared with the simulation value. The main reason for this difference is that the hardness and moisture content of the soil during the field test significantly affected the rotary tillage working resistance. This tillage performance evaluation index is within the acceptable range of agricultural machinery, confirming the reliability of the simulation model (Table 7).

Table 7.Analysis of variance of performance indicators

Test	Tillage Depth (mm)	Tillage Width (mm)	Experimental Resistance (N)	Simulated Resistance (N)	Unit soil mass （g）	Relative error/%
1	265.4	103.4	108.9	107.2	2531	1.59%
2	243.8	117.2	114.4	107.2	2780	6.72%
3	255.3	89.5	106.0	107.2	2151	1.12%
4	242.1	85.8	114.6	107.2	2304	6.90%
5	258.9	120.2	102.5	107.2	2369	4.38%
Mean	253.1	103.22	109.28	107.2	2427	1.94%

4. Conclusions

This study mainly designed and optimized a rotary tiller for tobacco fields, combined with bionic principles and numerical simulations to improve performance. A bionic curve, derived from the dung beetle foreleg, was applied to the rotary tiller blade, significantly enhancing soil cutting and throwing efficiency. A discrete element model (EDEM) was developed to simulate soil conditions in the tobacco fields, and the simulation results could accurately predict the

soil-tool interactions. Finite element analysis confirmed the blade's durability under extreme conditions, while the response surface methodology (RSM) optimized key operational parameters. The optimal configuration (350 rpm rotational speed, 0.4 m/s forward speed, and bionic blade type 5) achieved high performance in both simulation and field validation. The study validates the effectiveness of bionic design and DEM simulations in the development of high-performance agricultural machinery, providing valuable insights into future rotary tiller design in tobacco agriculture.

Author Contributions: Conceptualization, Ting Guo and **Wujin Li**; methodology, **Wujin Li**; software, **Shuguang Peng**; validation, **Shuguang Peng**; formal analysis, **Wen Li**; investigation, **Wen Li**; resources, **Shuguang Peng**; data curation, Ting Guo; writing— original draft preparation, Ting Guo; writing— review and editing, Ting Guo; visualization, **Xianglu Gong**; supervision, **Xianglu Gong**; project administration, **Wujin Li**; funding acquisition, **Wujin Li**; All authors have read and agreed to the published version of the manuscript.

Funding: This work was supported by the Science and technology project of Hunan Branch of China National Tobacco Corporation (HN2023KJ06).

Institutional Review Board Statement: Not applicable.

Informed Consent Statement: Not applicable.

Data Availability Statement: The original contributions presented in the study are included in the article, further inquiries can be directed to the corresponding author.

Conflicts of Interest: The authors declare that they have no known competing financial interests or personal relationships that could have appeared to influence the work reported in this paper.

References

1. Barnett, R., Peng, S., 2021. The Rise of China Tobacco: From Local to Global Player, in: Barnett, R., Yang, T., Yang, X.Y. (Eds.), Smoking Environments in China : Challenges for Tobacco Control. 2.Springer International Publishing, Cham, pp. 69–110. https://doi.org/10.1007/978-3-030-76143-1_3
2. Bratley, P., Fox, B.L., Schrage, L.E., 2011. A Guide to Simulation. Springer Science & Business Media.
3. Brunetti, G., Šimůnek, J., Bautista, E., 2018. A hybrid finite volume-finite element model for the numerical analysis of furrow irrigation and fertigation. Computers and Electronics in Agriculture 150, 312–327. https://doi.org/ 10.1016/j.compag.2018.05.013
4. Cui, Si., Zhong, W., 2023. China and Economic Globalization in Ming-Qing Dynasties:Examming from Introduction and Export of Tobacco. JOURNAL OF NANJING UNIVERSITY (PHILOSOPHY, humanities and Social Sciences) 60, 133-146+159-160.
5. Hong, L., Yi, J., Xujun, Z., 2021. Theoretical Logic of the Cultivation of New Professional Farmers in Tobacco Planting Industry in the New Era. tob regul sci 7, 2613–2623. https://doi.org/10.18001/TRS.7.5.1.31
6. Johnson, K.L., Kendall, K., Roberts, A.D., Tabor, D., 1997. Surface energy and the contact of elastic solids. Proceedings of the Royal Society of London. A. Mathematical and Physical Sciences 324, 301–313. https: //doi.org/10.1098/rspa.1971.0141
7. Mäeots, M., Pedaste, M., Sarapuu, T., 2008. Transforming Students' Inquiry Skills with Computer-Based Simulations, in: 2008 Eighth IEEE International Conference on Advanced Learning Technologies. Presented at the 2008 Eighth IEEE International Conference on Advanced Learning Technologies, pp. 938–942. https://doi.org/10.1109/ICALT.2008.239
8. Mudarisov, S.G., Gabitov, I.I., Lobachevsky, Y.P., Mazitov, N.K., Rakhimov, R.S., Khamaletdinov, R.R., Rakhimov, I.R., Farkhutdinov, I.M., Mukhametdinov, A.M., Gareev, R.T., 2019. Modeling the technological process of tillage. Soil and Tillage Research 190, 70–77. https://doi. org/10.1016/j.still.2018.12.004
9. National Bureau of Statistics of China, 2024. China Statistical Yearbook—2024.
10. Qian, Y., Zhu, Y., Ye, M., Huang, J., Wu, J., 2021. Experiment and numerical simulation for designing layout parameters of subsurface drainage pipes in arid agricultural areas. Agricultural Water Management 243, 106455. https://doi.org/10.1016/j.agwat.2020.106455
11. Tekeste, M.Z., Way, T.R., Syed, Z., Schafer, R.L., 2020. Modeling soil-bulldozer blade interaction using the discrete element method

(DEM). Journal of Terramechanics 88, 41–52. https://doi.org/10.1016/j.jterra.2019.12.003
12. Ucgul, M., Saunders, C., 2020. Simulation of tillage forces and furrow profile during soil-mouldboard plough interaction using discrete element modelling. Biosystems Engineering 190, 58–70. https://doi.org/10.1016/j.biosystemseng.2019.11.022
13. Wang, L., Xing, J., He, X., Li, X., Guo, W., Wang, X., Hou, S., 2023. Study on the Mechanism of Motion Interaction between Soil and a Bionic Hole-Forming Device. Agriculture 13, 1421. https://doi.org/10.3390/agriculture13071421
14. XIAO Maohua, W.K., 2021. Design and Experiment of Bionic Rotary Blade Based on Claw Toe of Gryllotalpa orientalis Burmeister. Transactions of the Chinese societyfor Agricultural Machinery 52, 55–63. https://doi.org/10.6041/j.issn.1000-1298.2021.02.005
15. Xiao, Q., Zhao, W., Ju, C., Peng, K., Yuan, M., Tan, Q., He, R., Huang, M., 2024. Effects of Different Tillage Depths on Soil Physical Properties and the Growth and Yield of Tobacco in the Mountainous Chongqing Region of China. Agriculture 14, 276. https://doi.org/10.3390/agriculture14020276
16. Zhong, W., Cui, Si., 2020. The Spread and Impact of Tobacco in China in the Context of Modern Globalization. seeking truth 47, 157-170+181. https://doi.org/10.19667/j.cnki.cn23-1070/c.2020.03.016
17. Zhu, D., Shi, M., Yu, C., Yu, Z., Kuang, F., Xiong, W., Xue, K., 2023. Tool-straw-paddy soil coupling model of mechanical rotary-tillage process based on DEM-FEM. Computers and Electronics in Agriculture 215, 108410. https://doi.org/10.1016/j.compag.2023.108410
18. Zhu, H., Wang, D., He, X., Shang, S., Zhao, Z., Wang, H., Tan, Y., Shi, Y., 2022. Study on Plant Crushing and Soil Throwing Performance of Bionic Rotary Blades in Cyperus esculentus Harvesting. Machines 10, 562. https://doi.org/10.3390/machines10070562